The SynCAM synaptic cell adhesion molecules are involved in sensory axon pathfinding by regulating axon-axon contacts

Frei, Jeannine A ; Andermatt, Irwin ; Gesemann, Matthias ; Stoeckli, Esther T

Abstract: Synaptic cell adhesion molecules (SynCAMs) are crucial for synapse formation and plasticity. However, we have previously demonstrated that SynCAMs are also required during earlier stages of neural circuit formation because SynCAM1 and SynCAM2 (also known as CADM1 and CADM2, respectively) are important for the guidance of post-crossing commissural axons. In contrast to the exclusively homophilic cis-interactions reported by previous studies, our previous in vivo results suggested the existence of heterophilic cis-interactions between SynCAM1 and SynCAM2. Indeed, as we show here, the presence of homophilic and heterophilic cis-interactions modulates the interaction of SynCAMs with trans-binding partners, as observed previously for other immunoglobulin superfamily cell adhesion molecules. These in vitro findings are in agreement with results from in vivo studies, which demonstrate a role for SynCAMs in the formation of sensory neural circuits in the chicken embryo. In the absence of SynCAMs, selective axon-axon interactions are perturbed resulting in aberrant pathfinding of sensory axons.

DOI: https://doi.org/10.1242/jcs.157032

© 2014. Published by The Company of Biologists Ltd | Journal of Cell Science (2014) 127, 5288–5302 doi:10.1242/jcs.157032

RESEARCH ARTICLE

The SynCAM synaptic cell adhesion molecules are involved in sensory axon pathfinding by regulating axon–axon contacts

Jeannine A. Frei, Irwin Andermatt, Matthias Gesemann and Esther T. Stoeckli*

ABSTRACT

Synaptic cell adhesion molecules (SynCAMs) are crucial for synapse formation and plasticity. However, we have previously demonstrated that SynCAMs are also required during earlier stages of neural circuit formation because SynCAM1 and SynCAM2 (also known as CADM1 and CADM2, respectively) are important for the guidance of post-crossing commissural axons. In contrast to the exclusively homophilic cis-interactions reported by previous studies, our previous *in vivo* results suggested the existence of heterophilic cis-interactions between SynCAM1 and SynCAM2. Indeed, as we show here, the presence of homophilic and heterophilic cis-interactions modulates the interaction of SynCAMs with trans-binding partners, as observed previously for other immunoglobulin superfamily cell adhesion molecules. These *in vitro* findings are in agreement with results from *in vivo* studies, which demonstrate a role for SynCAMs in the formation of sensory neural circuits in the chicken embryo. In the absence of SynCAMs, selective axon–axon interactions are perturbed resulting in aberrant pathfinding of sensory axons.

KEY WORDS: SynCAM, CADM, Cis interaction, Immunoglobulin superfamily, *In ovo* RNAi, Neural circuit formation

INTRODUCTION

The synaptic cell adhesion molecules SynCAMs, also known as nectin-like molecules (NECLs) or cell adhesion molecules (CADMs), are a subgroup of the immunoglobulin superfamily of cell adhesion molecules (IgSF-CAMs). SynCAMs were identified based on their potential to trigger synapse formation (Biederer et al., 2002). More recently, a role of SynCAM1 has been found in synaptic plasticity and spatial learning (Robbins et al., 2010). In agreement with these findings in mice, mutations in SynCAM1 (also known as CADM1) have been linked to autism in humans (Fujita et al., 2010; Zhiling et al., 2008), and lack of SynCAM1 impairs social behavior in mice (Takayanagi et al., 2010). Although such deficits are largely associated with synaptic plasticity, there is evidence that earlier steps in neural circuit formation might also be compromised in patients diagnosed with autism or intellectual disability (Stoeckli, 2012).

In agreement with the idea that molecules involved in synaptogenesis and synaptic plasticity might also have functions in earlier steps of neural circuit formation, we previously analyzed the role of SynCAMs in axon guidance (Niederkofler et al., 2010). SynCAMs are expressed by dI1 commissural neurons and floorplate cells during axonal pathfinding. *In vivo* studies indicated that axonal SynCAM1 and SynCAM2, and floorplate SynCAM2, are required for midline crossing and the subsequent rostral turn of commissural axons in the developing chicken spinal cord. Silencing SynCAM2 in floorplate cells and silencing SynCAM1 or SynCAM2 in commissural dI1 neurons interferes with the correct navigation of their axons along the rostro-caudal axis. Our finding that downregulation of SynCAM2 in commissural neurons also induces pathfinding errors at the floorplate was surprising based on the absence of a significant homophilic trans-interaction of SynCAM2 (Fogel et al., 2007; Niederkofler et al., 2010). Therefore, we postulated that SynCAMs can also form cis-heterodimers in addition to the published cis-homodimers.

In the current study, we tested this hypothesis using SynCAM fusion proteins in *in vitro* interaction assays. Our results confirm the existence of heterologous cis-interactions and suggest that they have a modulatory role on trans-interactions. This in turn affects SynCAM localization on growth cones and axonal interaction patterns, which are the key to the formation of neural circuits. Our *in vivo* studies demonstrate that SynCAM interactions are required for axon–axon contacts in the dorsal root entry zone (DREZ) and proper pathfinding of sensory axons and their collaterals.

RESULTS

SynCAMs form homophilic and heterophilic cis- and trans-interactions

Results from our previous *in vivo* study suggested that SynCAM1–SynCAM2 hetero-cis-dimers exist on commissural dI1 axons (Niederkofler et al., 2010). In that study, we found that silencing SynCAM2 expressed by floorplate cells resulted in axonal pathfinding errors. The same navigation errors are seen after silencing SynCAM1 or SynCAM2 in dI1 neurons. Although the results obtained after blocking SynCAM1 can be explained by its strong heterophilic trans-interaction to floorplate SynCAM2, the finding that silencing axonal SynCAM2 also interfered with pathfinding was surprising, as homophilic SynCAM2 interactions have been found to be very weak (Fogel et al., 2007; Niederkofler et al., 2010). Thus, the most parsimonious explanation for the observed phenotype was the existence of heterophilic SynCAM1–SynCAM2 cis-dimers or cis-oligomers on dI1 axons.

To find evidence for heterophilic cis-interactions, we carried out binding assays with purified tagged ectodomains of SynCAM1 and SynCAM2 added to HeLa cells expressing full-length SynCAMs (Fig. 1). In line with previous studies (Fogel et al., 2007; Niederkofler et al., 2010), homophilic interactions were very weak in comparison to heterophilic interactions (Fig. 1A–D,G). These results were confirmed by co-immunoprecipitation studies with SynCAMs expressed in HEK293T cells, and SynCAMs

Institute of Molecular Life Sciences and Neuroscience Center Zurich, University of Zurich, Winterthurerstrasse 190, 8057 Zurich, Switzerland.

*Author for correspondence (esther.stoeckli@imls.uzh.ch)

Received 23 May 2014; Accepted 13 October 2014

Journal of Cell Science

Journal of Cell Science (2014) 127, 5288–5302 doi:10.1242/jcs.157032

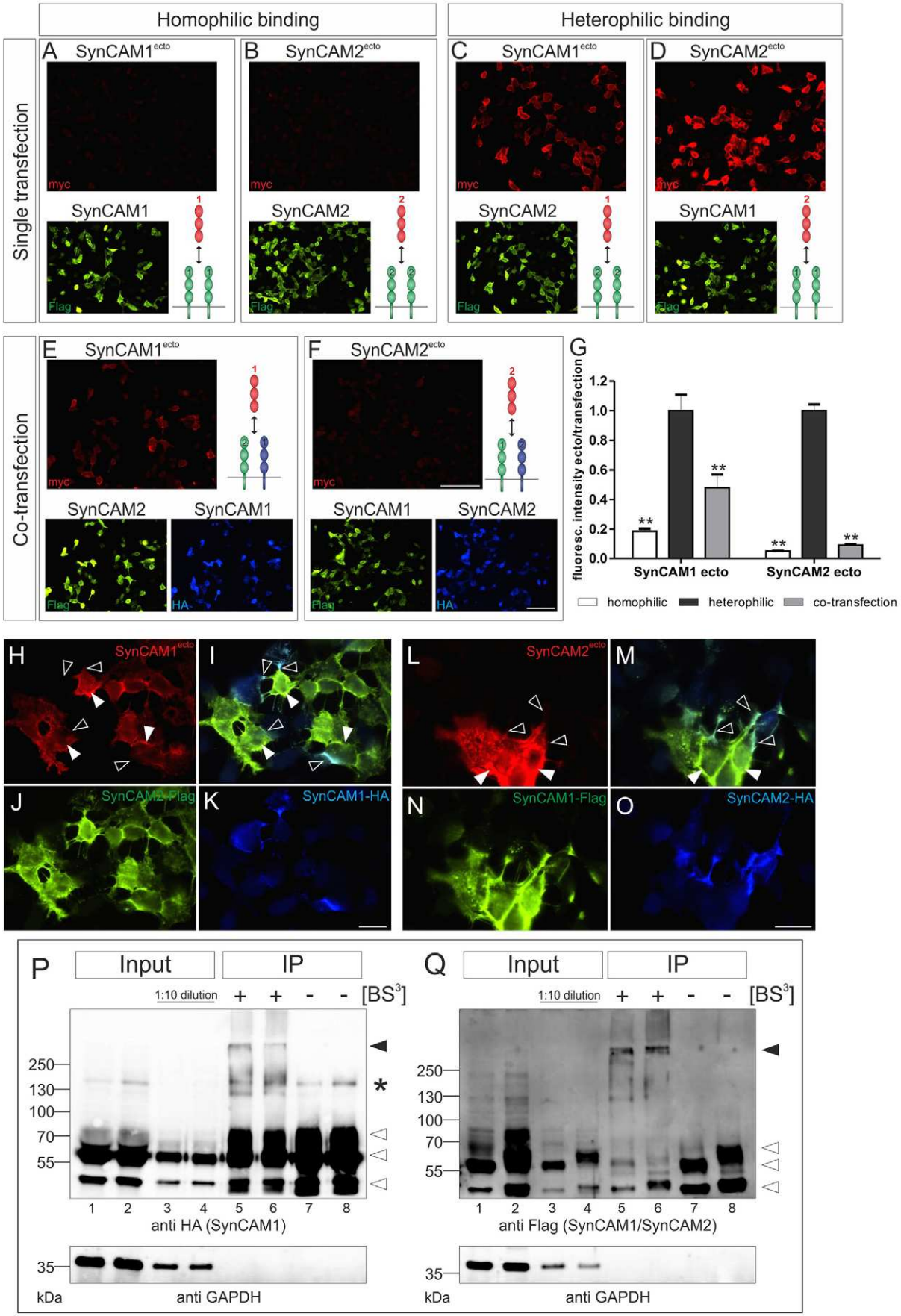

Fig. 1. See next page for legend.

Journal of Cell Science (2014) 127, 5288–5302 doi:10.1242/jcs.157032

Fig. 1. Heterophilic cis-complexes between SynCAM1 and SynCAM2 modify trans-binding. (A–G) SynCAM binding to cells co-transfected with both SynCAM1 and SynCAM2 is reduced. HeLa cells transfected with SynCAM1–Flag (A,D), SynCAM2–Flag (B,C), or co-transfected with both SynCAM1–HA and SynCAM2–Flag (E) and SynCAM1–Flag and SynCAM2–HA (F) were incubated with purified Myc-tagged SynCAM1 (A,C,E) or SynCAM2 ectodomains (ecto) (B,D,F). Homophilic binding of SynCAM1^{ecto} to SynCAM1 (A) and SynCAM2^{ecto} to SynCAM2 (B) was weak. In contrast, heterophilic binding of SynCAM1^{ecto} to SynCAM2 (C) and of SynCAM2^{ecto} to SynCAM1 (D) was strong. Binding of SynCAM1^{ecto} (E) and SynCAM2^{ecto} (F) to co-transfected cells was markedly reduced compared to heterophilic binding to singly transfected cells (C,D). Bound ectodomains were visualized with anti-Myc antibody (red), transfected full-length SynCAMs with anti-Flag (green) or anti-HA antibodies (blue). (G) Quantification of SynCAM1 and SynCAM2 ectodomain binding to singly transfected (homophilic binding white, heterophilic binding black bars) and co-transfected cells (gray). Note that SynCAM2 binding to co-transfected cells is reduced more strongly than SynCAM1 binding. $^{**}P<0.01$ for the comparison to heterophilic binding using ANOVA with Tukey's post-hoc test. Values are given as mean±s.e.m. One representative experiment out of five is shown in G. (H–O) Reduction in SynCAM binding to co-transfected cells is not an artifact due to the unavailability of binding partners on cell surfaces. Cells separately transfected with SynCAM2–Flag (J, green), SynCAM1–HA (K, blue), SynCAM1–Flag (N, green) or SynCAM2–HA (O, blue) were mixed (I,M) and incubated with SynCAMs (H,L, red). SynCAM1^{ecto} (H) was not able to compete with heterophilic SynCAM1–HA and SynCAM2–Flag interactions (compare black arrowheads in H and I). However, there was still SynCAM2–Flag on the cell membrane, which was not involved in the contact site and, thus, was available for SynCAM1^{ecto} binding (H,I, white arrowheads). The same was true for SynCAM2^{ecto} (L,M, white arrowheads). Scale bars: 100 μm (A–F); 25 μm (H–O). (P,Q) Cross-linking reveals heterophilic cis-interactions between SynCAM1 and SynCAM2. HEK293T cells were co-transfected with either SynCAM1–HA and SynCAM1–Flag (positive control) or SynCAM1–HA and SynCAM2–Flag. Single cells were incubated with the cross-linker BS^3 and lysates were submitted to immunoprecipitation (IP). Western blots were stained with anti-HA- (P) or anti-Flag-antibodies (Q). Input lysates were loaded undiluted (lanes 1 and 2) and 1:10 diluted (lanes 3 and 4). Lanes 5 and 7 represent the precipitate of the control reaction (homophilic SynCAM1 pulldown), lanes 6 and 8 represent the pulldown of SynCAM2 with SynCAM1 with (lanes 5 and 6) and without BS^3 (lanes 7 and 8). (P) In the presence of BS^3, SynCAM1–HA was pulled down using anti-HA-antibodies both in their monomeric form (arrowheads) and as multimeric complexes (black arrowhead; lane 5, 6). In the absence of BS^3, SynCAM1–HA was only present as monomer (open arrowheads; lanes 7 and 8). The band at 130 kDa (asterisk) could not be clearly identified and could represent either an unspecific band or SynCAM1 dimers. This band was not detected with the anti-SynCAM1 antibody in lysates of HEK293T cells overexpressing SynCAM1 (Fig. 1D, lane 4). (Q) SynCAM1–Flag (lane 5) and SynCAM2–Flag (lane 6) were present in the high molecular mass complexes (black arrowhead) with but not without BS^3 (lanes 7 and 8). GAPDH served as loading control.

endogenously expressed in 5-day-old chick dorsal root ganglia (DRG) explants (supplementary material Fig. S1). A relatively strong homophilic SynCAM1 interaction was detectable in our co-immunoprecipitation assays (supplementary material Fig. S1A) in contrast to cell-based binding assays (Fig. 1A). This discrepancy could be due to cis- rather than trans-interactions in the co-immunoprecipitation studies compared to in the cell-based assay.

In line with observations made for other IgSF-CAMs (Kunz et al., 1998), we speculated that heterophilic cis-interactions might alter the affinity for trans-interactions. To test this possibility, we co-transfected HeLa cells with both SynCAMs and incubated the cells with either SynCAM1 or SynCAM2 ectodomains (Fig. 1E,F). Binding of SynCAM1^{ecto} to cells expressing both SynCAMs was reduced by 52% compared to binding to cells transfected with SynCAM2 alone (Fig. 1E,G). An even stronger reduction by 91% was observed for SynCAM2^{ecto} trans-binding to cells expressing both SynCAMs compared to cells transfected with SynCAM1 alone (Fig. 1F,G). Taken together, our *in vitro* binding studies demonstrate that the presence of both SynCAM1 and SynCAM2 in the cell membrane reduces, or even inhibits, the binding of SynCAM ectodomains, suggesting that the formation of heterophilic SynCAM1–SynCAM2 cis-clusters weakens the trans-binding of SynCAMs compared to homophilic cis-clusters.

To rule out the possibility that the observed reduction of SynCAM trans-binding to co-transfected cells was caused by the unavailability of binding partners on the cell surface owing to their recruitment through heterophilic interactions at cell–cell contact sites, we carried out another series of binding studies. HeLa cells were separately transfected with HA- and Flag-tagged SynCAM1 and SynCAM2, respectively, mixed and incubated with SynCAM1 or SynCAM2 (Fig. 1H–O). At the concentrations used in our binding assays, the soluble SynCAM ectodomains added to the cultures were not able to compete with cell surface SynCAMs engaged in heterophilic cell–cell contact sites (black arrowheads in Fig. 1H,I,L,M). However, they still bound to SynCAMs, which were not recruited to these contact sites (white arrowheads in Fig. 1H,I,L,M). Thus, the reduced amount of trans-interactions was not due to the absence of SynCAM-binding partners on the cell surface at non-contact sites.

Additional evidence for the existence of heterophilic SynCAM1–SynCAM2 cis-interactions was obtained by cross-linking experiments (Fig. 1P,Q). We added bis-sulfosuccinimidyl suberate (BS^3), an 11-Å-long cross-linker, to cells co-transfected with SynCAM1–HA and SynCAM1–Flag, and SynCAM1–HA and SynCAM2–Flag. Co-transfection of SynCAM1–HA and SynCAM1–Flag served as a positive control because SynCAM1 is known to form homophilic cis-complexes (Fogel et al., 2011). To make sure that trans-interactions did not confound our results, we re-plated transfected cells at low density. Indeed, SynCAM1–HA and SynCAM1–Flag, as well as SynCAM1–HA and SynCAM2–Flag were successfully cross-linked into oligomers (Fig. 1P,Q, lanes 5 and 6).

Taken together, these findings confirm the presence of SynCAM1–SynCAM2 heterophilic cis-interactions. Furthermore, our results suggest that hetero-cis-clusters modulate the binding preferences in trans because trans-binding of SynCAM1 and SynCAM2 to heterophilic cis-clusters was strongly reduced or virtually abolished when compared to homophilic cis-clusters.

SynCAMs are expressed in DRG sensory neurons throughout development

In line with our findings in commissural axon navigation (Niederkofler et al., 2010), we found that SynCAMs were expressed in sensory and motor neurons during hindlimb innervation of the chicken embryo (Fig. 2). SynCAM1 mRNA was already expressed in somites at Hamburger and Hamilton (HH) stage 11 (Fig. 2A). At HH18, when the DRG starts to form, we detected both SynCAM1 and SynCAM2 mRNA expression, and all three SynCAMs were expressed in motoneurons (data not shown). Starting at HH21, all three SynCAM mRNAs were present in DRG (Fig. 2D–I). At HH30 and HH34, SynCAMs were expressed in a subtype-specific manner in DRG neurons. In chicken, like in human, subpopulations of sensory neurons are segregated to different positions in the DRG (Eide and Glover, 1997). SynCAM1 mRNA (Fig. 2J) was restricted to the dorsomedial region, colocalizing with TrkA (also known as NTRK1)-positive neurons, whereas SynCAM2 (Fig. 2K) was

Journal of Cell Science (2014) 127, 5288–5302 doi:10.1242/jcs.157032

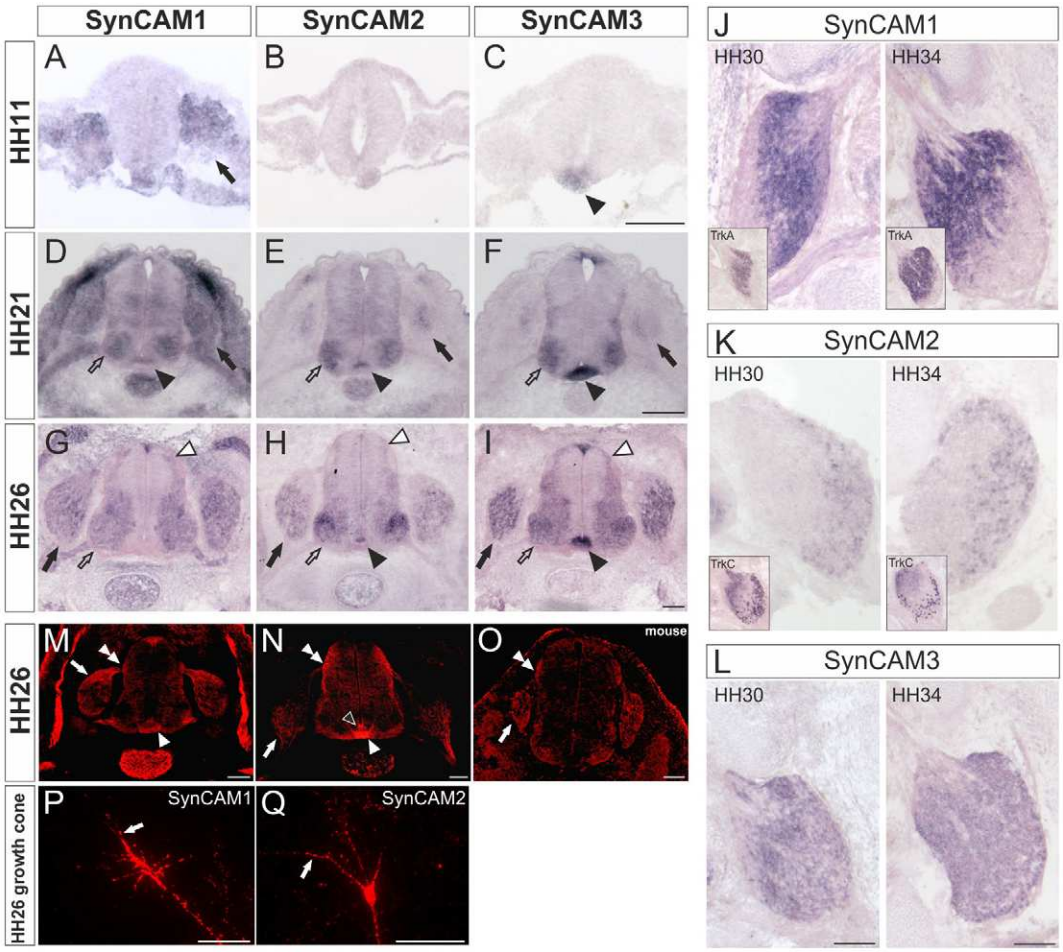

Fig. 2. SynCAMs are expressed in DRG sensory neurons. (A) At stage HH11, SynCAM1 mRNA was found in somites (black arrow), SynCAM2 was not yet expressed (B), and SynCAM3 was found only in the floorplate (C, black arrowhead). By HH21 (D–F), all SynCAMs were expressed in DRG (black arrows), in motoneurons (open arrows) and in the floorplate (black arrowheads). SynCAMs were still present in the DRG and motoneurons at HH26 (G–I, arrows). SynCAM1 (G) was no longer found in the floorplate, in contrast to SynCAM2 (H, black arrowhead) and SynCAM3 (I, black arrowhead). SynCAMs were now also expressed in commissural neurons in the dorsal spinal cord (G-I, white arrowheads). At HH30 and HH34, SynCAM1 (J) and SynCAM2 (K) expression was restricted to the dorsomedial and the ventrolateral region of the DRG, respectively. In chick, unlike in rodents, where neurons are arranged randomly, subpopulations of sensory neurons are segregated to different domains of the DRG (Eide and Glover, 1997). Insets depict staining for TrkA (J) and TrkC (K). Note that SynCAM1 and TrkA as well as SynCAM2 and TrkC are found in similar regions of the DRG. SynCAM3 showed a more widespread expression at stage HH30 and HH34 DRG (L). (M-O) Immunostaining of SynCAM1 (M) and SynCAM2 (N) on HH26 chicken spinal cord sections confirmed expression in the dorsomedial and ventrolateral DRG (arrows), respectively, in the dorsal root (double arrowheads), in the commissure and on post-crossing commissural axons in the ventral spinal cord (white arrowheads). SynCAM2 was also found in the floorplate (N, arrowhead). The antibody against human SynCAM3 recognized SynCAM3 in DRG (arrow) and sensory axons (double arrowhead) in mouse spinal cord sections (O). (P,Q) SynCAM1 (P) and SynCAM2 (Q) were present on the surface of axons and growth cones of sensory neurons. Note the strong staining of filopodia (arrows). Neurons were stained before fixation to detect surface-expressed proteins only. Scale bars: 100 μm (A–O); 20 μm (P,Q).

mainly found in ventrolaterally located neurons, colocalizing with TrkC (also known as NTRK3)-positive cells. Between HH30 and HH34, SynCAM3 was found throughout the DRG, although at different expression levels (Fig. 2L).

In line with the mRNA distribution, SynCAM1 protein was found mainly in the dorsomedial DRG and on sensory axons (Fig. 2M). Strong immunoreactivity was also observed in the roof plate and on commissural axons, both in the commissure and on post-crossing axons, in the notochord and in the dermomyotome. SynCAM2 immunoreactivity was observed in the DRG, most strongly in the ventrolateral part, and on sensory axons (Fig. 2N). Commissural axons, both in the commissure and in the longitudinal axis, were positive for SynCAM2. In contrast to SynCAM1, SynCAM2 was found in the floorplate, in line with the *in situ* hybridization results. The antibody against human SynCAM3 did not specifically recognize chicken SynCAM3 (data not shown). Staining of mouse tissue confirmed expression in DRG and motor neurons but failed to detect SynCAM3 in the floorplate (Fig. 2O).

To investigate whether SynCAM1 and SynCAM2 were also expressed on growth cones, we cultured dissociated sensory neurons of 5-day-old chicken embryos on laminin. Staining of unfixed cells after 2 days *in vitro* revealed that both SynCAM1 (Fig. 2P) and SynCAM2 (Fig. 2Q) were present on the surface of sensory axons and growth cones with prominent expression on filopodia. In summary, our expression studies localize SynCAMs to DRG sensory neurons throughout neural circuit development.

SynCAMs mediate adhesion of sensory axons

In a first step towards understanding the function of SynCAMs, we demonstrated an adhesive effect of SynCAMs on DRG

Journal of Cell Science (2014) 127, 5288–5302 doi:10.1242/jcs.157032

sensory neurons in an *in vitro* choice assay (supplementary material Fig. S2A,D). We found significantly more growth cones on SynCAM-expressing cells compared to control-transfected cells. For neurons dissected from E5 embryos, we found 4.6-fold more growth cones on SynCAM1-expressing cells, 3.7-fold more on SynCAM2-expressing cells and 3.5-fold more on SynCAM3-expressing cells compared to cells transfected with MARCKS–GFP (supplementary material Fig. S2E). Similar values were found for neurons of E8 embryos, with 3.2-fold, 2.7-fold, and 2.2-fold more growth cones on SynCAM1-, SynCAM2- and SynCAM3-transfected cells, respectively (supplementary material Fig. S2F). Thus, growth cones showed a strong preference for SynCAM-expressing cells.

SynCAMs induce neurite outgrowth of old but not young sensory neurons

IgSF-CAMs have been shown to promote neurite growth of sensory neurons (Buchstaller et al., 1996; Kuhn et al., 1991; Lustig et al., 1999; Morales et al., 1993; Stoeckli et al., 1991; Stoeckli et al., 1996). To test whether this was also true for the SynCAM subgroup, we cultured dissociated sensory neurons dissected from 5- and 8-day-old embryos at low density on SynCAM and control substrates. Neurite lengths were measured at 28 and 48 hours after plating the cells on three different concentrations of purified SynCAM ectodomains (Fig. 3). Total axonal length of E5 sensory neurons cultured on 50 µg/ml SynCAM substrates was similar to those on poly-lysine substrates (Fig. 3A–C). For the longest axon per neuron, there was a trend to higher values on SynCAMs, although values for SynCAM3 were not significant (Fig. 3B; supplementary material Table S1A).

In contrast, SynCAM substrates significantly promoted elongation of sensory axons dissected from E8 embryos (Fig. 3D–H). SynCAM2 and SynCAM3 promoted neurite outgrowth in a dose-dependent manner (Fig. 3H). On high and low substrate concentrations both the longest neurites (Fig. 3E,G; supplementary material Table S1B) and total neurite lengths (Fig. 3D,F; supplementary material Table S1B) were significantly longer on SynCAM2 and SynCAM3 compared to poly-lysine. The effect of SynCAM1 on neurite outgrowth was weaker and not concentration-dependent.

For E8 sensory neurons analyzed 28 hours after plating, total axon length as well as the length of the longest axon per neuron were significantly increased on all SynCAMs compared to poly-lysine (Fig. 3I,J; supplementary material Table S1C) but independent of the coated concentration (Fig. 3K). Taken together, SynCAMs have a neurite-outgrowth-promoting effect on E8, but not on, E5 sensory axons. The effect is dose dependent but only after an extended growth period. Thus, we conclude that SynCAMs do not primarily affect axon elongation.

SynCAMs mediate selective axon–axon contacts

More striking than the small, but significant, effect on neurite outgrowth were changes in axonal morphology (Fig. 4). The number of filopodia along axons was 1.6-fold higher on SynCAM1 compared to poly-lysine (Fig. 4A,G). Values on SynCAM2 (Fig. 4B,G) and SynCAM3 (Fig. 4C,G) were 1.4- and 1.5-fold higher. Moreover, more filopodia along axons grown on SynCAM substrates tended to be branched compared to filopodia on poly-lysine, Albumax and laminin, although only the comparison with Albumax was statistically significant (Fig. 4H).

Most strikingly, neurites extending from DRG explants cultured on SynCAM substrate formed highly disorganized networks (supplementary material Fig. S3A–F; Fig. 4O–R). Instead of radial axon bundles, as seen on control substrates, axonal bundles on SynCAMs were highly interconnected by axons that crossed between bundles. We next compared the morphology of axonal networks extending from DRG explants lacking SynCAMs with control DRG on collagen (supplementary material Fig. S3G–K). Similarly, we found striking differences in axonal behavior also under these conditions. Again, we observed a large number of neurites crossing between axon bundles in the absence of any one of the SynCAMs, along with a marked increase in filopodia number, resulting in a highly disorganized appearance of the axonal network. This was no different when we used SynCAM substrates rather than collagen (Fig. 4I–L). However, when we cultured DRG neurons lacking both SynCAM1 and SynCAM2 on a SynCAM substrate growth morphology was clearly different and resembled much more the morphology observed on control substrates, indicating that axon growth under these conditions might no longer depend on SynCAMs (Fig. 4M,N).

Taken together, axonal network morphology was changed when DRG were grown on SynCAM compared to control substrates. Similar changes were observed after knockdown of SynCAMs in DRG neurons grown on collagen or SynCAMs. Thus, it does not matter in what direction the balance between the different SynCAMs is tipped; too much or too little of any SynCAM results in disruption of normal axon–axon contacts.

SynCAM substrates affect growth cone morphology and SynCAM distribution on the growth cone surface

The observed changes in axon–axon contact in DRG explant cultures were reflected by changes in growth cone morphology. On SynCAM substrates, growth cones were significantly larger (Fig. 5A–G). The average surface area of growth cones on SynCAM1 was 396.6 μm^2, 799.7 μm^2 on SynCAM2 and 575.9 μm^2 on SynCAM3, compared to 133.8 μm^2 on laminin, 149.1 μm^2 on Albumax and 244.7 μm^2 on poly-lysine. When we analyzed the number of filopodia, normalized to the perimeter of the growth cones, we did not find a significant difference between control substrates and SynCAMs, with the exception of SynCAM2, where we found a minor decrease in the number of filopodia when compared to the number of filopodia from growth cones on poly-lysine (data not shown). Thus, in marked contrast to the increase in filopodia number along axons, the number of filopodia on growth cones did not differ significantly compared to control substrates.

However, significant differences were found, when we compared growth cone morphologies. We categorized growth cones into different shape groups: round, thin and branched, long and thin, and long and flat (Fig. 5H). On SynCAM2 substrate, 77% of the growth cones were classified as round and 23% as long and flat, whereas growth cones on SynCAM1 (54%) and SynCAM3 (60%) were mostly round, or thin and branched (26% and 27%, respectively). Growth cones on poly-lysine were mostly round (53%) or had a thin and branched shape (35%), similar to growth cones on SynCAM1 and SynCAM3, although growth cones on poly-lysine were much smaller. The majority of the growth cones on laminin (51%) and Albumax (54%) were thin and branched. These results indicate that growth cones respond differently to SynCAM substrates, reflected by specific changes in size and shape.

Because growth cone morphologies differed between SynCAM substrates, we tested whether SynCAMs were actively involved

Journal of Cell Science (2014) 127, 5288–5302 doi:10.1242/jcs.157032

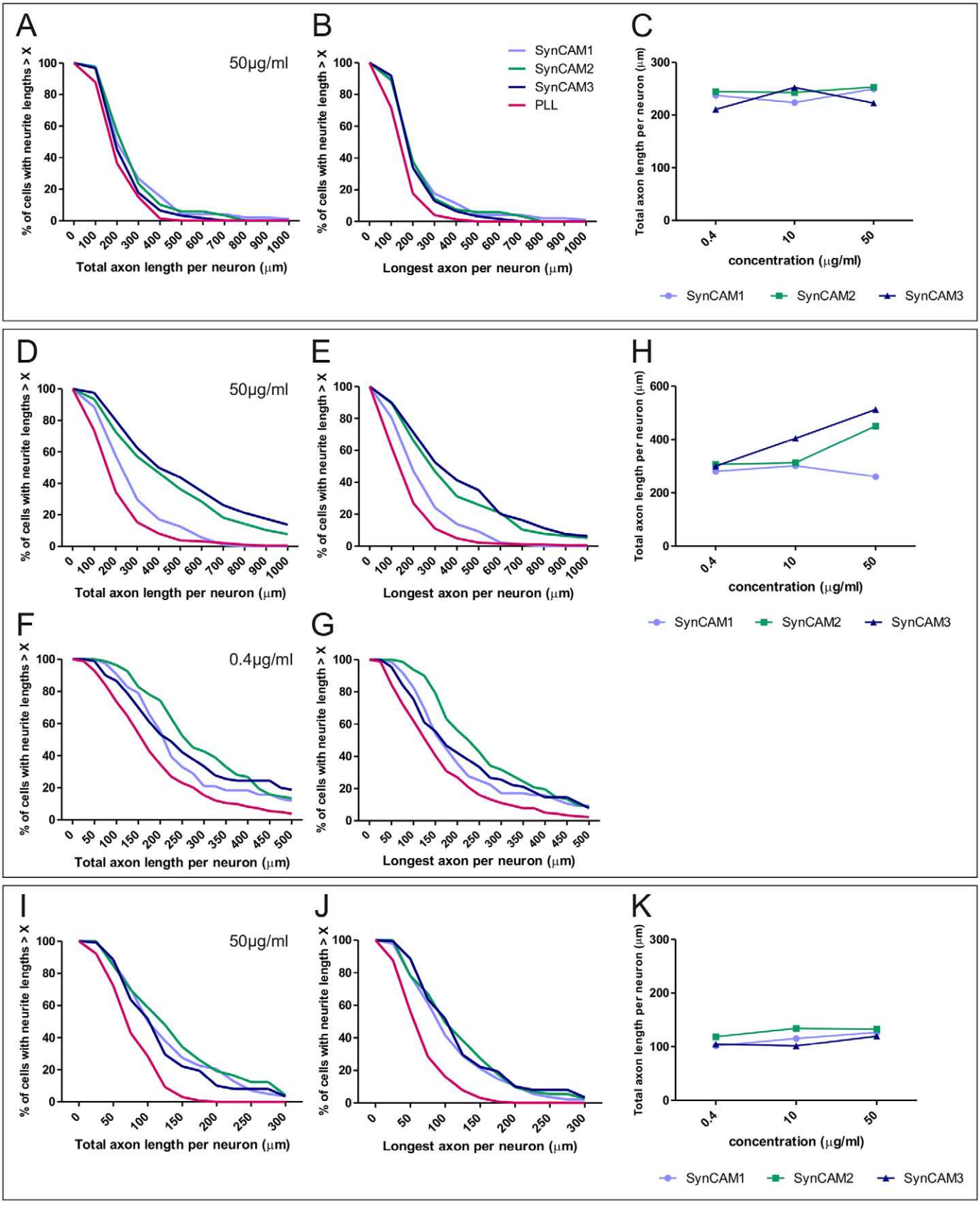

Fig. 3. See next page for legend.

Journal of Cell Science (2014) 127, 5288–5302 doi:10.1242/jcs.157032

Fig. 3. SynCAMs promote neurite outgrowth of E8 but not of E5 sensory neurons. Dissociated sensory neurons of E5 (A-C) and E8 embryos (D-K) were cultured on substrates containing 50 μg/ml (A–E, H–K) or 0.4 μg/ml (F,G) SynCAM1, SynCAM2 or SynCAM3. Axons were grown for 48 (A–H) or 28 hours (I–K). Total axon lengths of neurons dissected from E5 embryos on 50 μg/ml SynCAM substrates did not significantly differ from poly-lysine (A; supplementary material Table S1A). The longest neurites per neuron were slightly but significantly longer on SynCAM1 and SynCAM2 compared to poly-lysine (B; supplementary material Table S1A). Neurite growth of E5 sensory axons was not concentration-dependent (C). (D–G) For E8 sensory neurons, the total axon length (D,F) was significantly longer on all SynCAM concentrations (supplementary material Table S1B). Longest neurites (E,G) were also longer for SynCAMs, except SynCAM1, where values were not significantly different from poly-lysine for some concentrations. The growth-promoting effect of SynCAM2 and SynCAM3, but not of SynCAM1, was concentration-dependent (H). (I–K) E8 axons grown for only 28 hours showed significantly longer total axon length (I) and length of the longest axon per neuron (J) on 50 μg/ml SynCAM substrate compared to poly-lysine. In contrast to growth for 48 hours (H), the outgrowth-promoting effect was independent of the substrate concentration during the first 28 hours (K, supplementary material Table S1C). Mean values and statistical significances are given in supplementary material Table S1. Values represented in the plots were taken from one representative experiment out of three for E8. One experiment with E5 neurons is represented. At least 70 neurons per condition were used for quantification.

in the contact between the growth cone and the substrate. To this end, we compared surface staining of SynCAM1 and SynCAM2 on sensory growth cones. Live staining of axons grown on SynCAM1 (Fig. 5I,L) and SynCAM2 substrate (Fig. 5J,M) showed that SynCAM1 was cleared from the apical growth cone surface (Fig. 5I′,J,J′). Similarly, SynCAM2 was depleted from the apical surface on both SynCAM1 (Fig. 5L,L′) and SynCAM2 substrate (Fig. 5M,M′). In contrast, both SynCAM1 (Fig. 5K,K′) and SynCAM2 (Fig. 5N,N′) were readily detected on the apical growth cone surface on laminin. Thus, SynCAMs were depleted from the apical surface and relocated to the substrate-facing surface of the growth cone in a substrate-dependent manner. On laminin, where axons grow in an integrin-dependent manner, SynCAMs are not recruited to the substrate-facing surface of the growth cone.

Taken together, the changes in growth cone morphology and the redistribution of SynCAMs to the substrate-facing membrane suggests that there is an active contribution of these molecules to growth-cone–substrate contacts. More generally, these observations reflect an active role of SynCAMs in selective axon–axon contacts of sensory neurons.

SynCAMs are required for the proper spinal cord entry of sensory afferents

A good *in vivo* model to test the suggested role of SynCAMs in the regulation of axon–axon contacts during sensory neural circuit formation is the entry of sensory axons into the spinal cord at the dorsal root entry zone (DREZ). There, axons need to select between a more ventral and a more dorsal pathway along the longitudinal axis of the spinal cord. Thereby they reach the appropriate position in the dorsal funiculus, from where they extend collaterals (Eide and Glover, 1995; Perrin et al., 2001). In this longitudinal bundle, axons sort out depending on their sensory modality. Proprioceptive axons bifurcate in a rather Y-shaped manner to reach the dorsomedial funiculus, whereas nociceptive axons extend in a T-shaped manner, as they form collaterals from the lateral funiculus (Perrin et al., 2001).

We used *in ovo* RNA interference (RNAi) to perturb SynCAM expression in DRG. First, we analyzed trajectories of sensory axons in whole-mount preparations of E5 (HH24.5 or HH25) embryos stained for neurofilaments (Fig. 6A–F). Loss of any SynCAM resulted in abnormal entry of sensory afferents into the dorsal spinal cord. Aberrant sensory afferent entry was seen in 25% of the embryos lacking SynCAM1 (Fig. 6A,E), in 37% of the embryos lacking SynCAM2 (Fig. 6B,E), and in 36% of the embryos lacking SynCAM3 (Fig. 6C,E). This was rarely found in control embryos, with only 8% aberrant bundles found for both control-treated and untreated embryos (Fig. 6D,E). In contrast to control embryos, the longitudinal sensory axon bundle had a wavy appearance in the absence of SynCAMs. The ratio of bundle thickness measured between two DRG and at root entry sites was significantly reduced in experimental compared to control embryos (Fig. 6F). This effect was not due to cell survival, as downregulation of SynCAMs did not change the number of cells in the DRG (data not shown).

To find an explanation for the aberrant morphology of the longitudinal axon bundle, we looked at the DREZ in cross-sections of the spinal cord (Fig. 6G–I). Knockdown of SynCAM2 and SynCAM3 resulted in segmentation of the axon bundle, which was visualized by antibodies against axonin1 (also known as contactin 2). Instead of the smooth oval shape of the DREZ and the regular arrangement of axons seen in control embryos (Fig. 6I,J), we found gaps and an aberrant shape of the axon bundle in 33% of embryos lacking SynCAM2 (Fig. 6G,J) and in 38% of embryos lacking SynCAM3 (Fig. 6H,J). Downregulation of SynCAM1 had no effect, as segmented sensory axon bundles were only observed in 19% of the embryos (Fig. 6J). This was not significantly different from control-treated (11%) and untreated embryos (13%). In summary, silencing SynCAMs resulted in aberrant sensory axon pathfinding in the DREZ.

We next checked whether the wavy appearance of the longitudinal axon bundle was caused by aberrant bifurcation of sensory afferents in the DREZ (supplementary material Fig. S4). The injection of DiI into the DRG of control embryos revealed two distinct bundles, forming a T- and a Y-shaped trajectory. Although sensory axons also bifurcated in the DREZ in the absence of SynCAMs, the T- and Y-shaped trajectories were not clearly defined, as axons bifurcated with more random angles resulting in a diffuse appearance of the DREZ.

Taken together, these findings are consistent with our *in vitro* analyses and suggest that SynCAMs are required for selective axon–axon contacts, which in turn contribute to correct pathfinding of sensory axons along the longitudinal axis of the spinal cord.

SynCAMs are involved in layer-specific targeting of sensory collaterals in the gray matter

Because SynCAM mRNAs were expressed in a subpopulation-specific manner in DRG at later stages (Fig. 2J–L; Fig. 7A,B), we analyzed whether SynCAMs were involved in pathfinding of sensory collaterals into the gray matter of the spinal cord. SynCAM1 was enriched in the lateral funiculus and in collaterals projecting horizontally in the dorsal horn of the spinal cord, suggestive of expression in nociceptive fibers (Fig. 7A). In contrast, SynCAM2 was absent from these regions but expressed in the medial funiculus, where proprioceptive afferents are found (Fig. 7B). To investigate the pathfinding of sensory collaterals we stained vibratome slices of control and experimental embryos

Journal of Cell Science (2014) 127, 5288–5302 doi:10.1242/jcs.157032

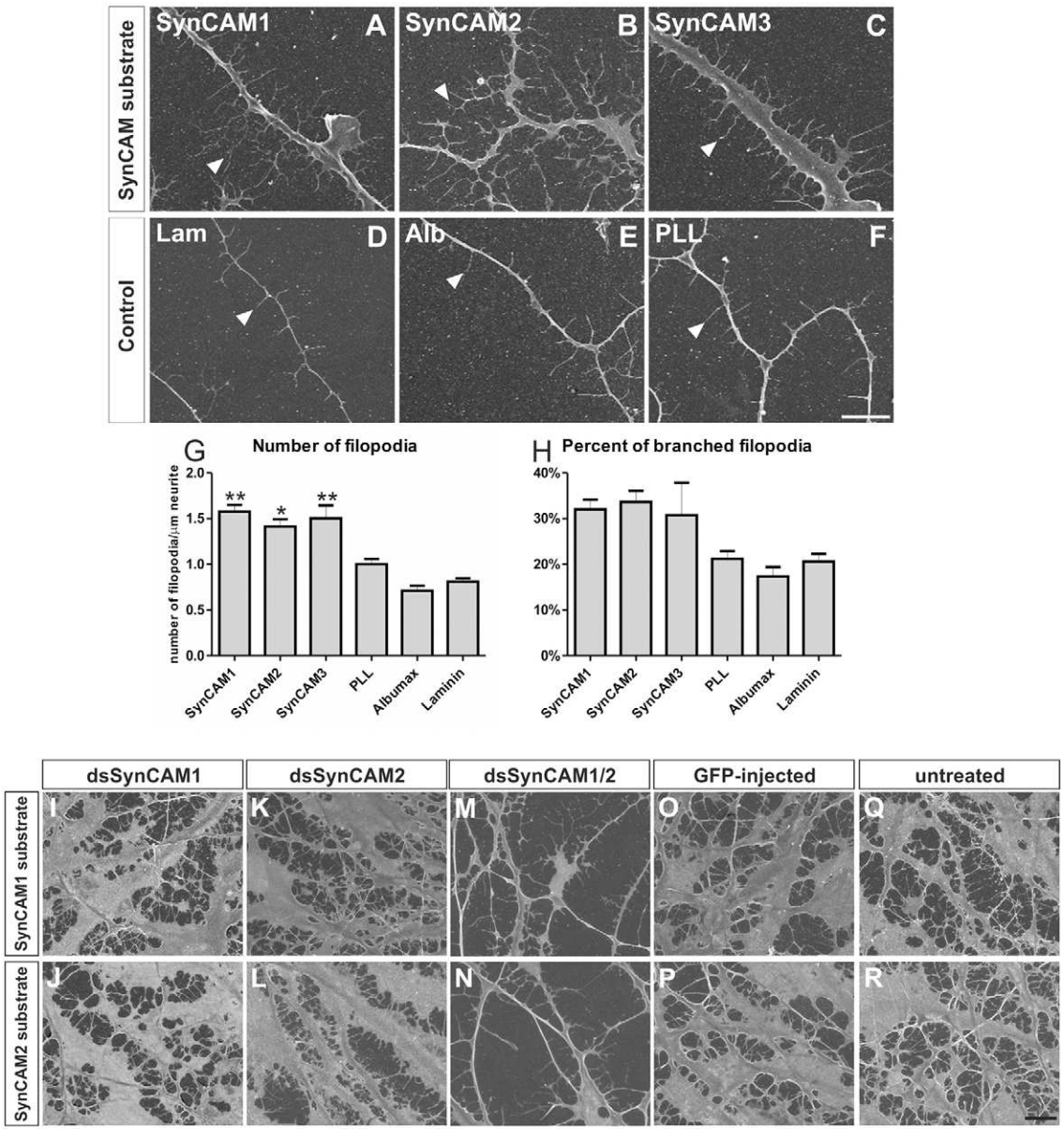

Fig. 4. SynCAMs mediate selective axon–axon contacts by homophilic and heterophilic interactions. Scanning electron micrographs of single axons grown from DRG explants cultured on SynCAM1 (A), SynCAM2 (B) SynCAM3 (C), laminin (D), Albumax (E) and poly-lysine (F). On SynCAMs (A–C) axons produced more filopodia (arrowheads) compared to the control substrates (D–F). Significantly more filopodia per μm of neurite (G) and more branched filopodia (H) were seen on SynCAMs compared to control substrates. Between 27 and 90 neurites per condition were quantified, except for SynCAM3, where *n* was only five due to the fact that single neurites were virtually absent. **P*<0.05, ***P*<0.01 for the comparison between SynCAMs and poly-lysine (G) using ANOVA with Tukey's post-hoc test. Values are given as mean±s.e.m. Scanning electron micrographs taken from the peripheral axonal network of DRG explants lacking SynCAM1 (I,J), SynCAM2 (K,L), or both SynCAM1 and SynCAM2 (M,N) were compared to images from control-treated (O,P) and untreated (Q,R) DRG grown on either SynCAM1 (I,K,M,O,Q) or SynCAM2 substrate (J,L,N,P,R). Morphology and growth behavior of sensory axons was similar for all conditions, except the double-knockdowns. Scale bar: 10 μm.

killed at E9 (HH35) for axonin1, a marker for nociceptive neurons, and for the RT97 epitope, a marker for proprioceptive neurons. We found a significantly increased number of embryos with aberrant projections of axonin1-positive collaterals after downregulation of SynCAM2 and SynCAM3 and a tendency to more pathfinding errors after knockdown of SynCAM1 (Fig. 7C). Significantly more RT97-expressing collaterals showed aberrant projections into the gray matter of the spinal cord when SynCAM2 levels were reduced (Fig. 7D). Nociceptive collaterals, which normally extend from the lateral dorsal funiculus into laminae I and II of the dorsal horn (Eide and Glover, 1997; Perrin et al., 2001), were found to overshoot their target and project to lamina III, or even to cross the midline (Fig. 7E–G). In control embryos, collaterals correctly targeted laminae I and II (Fig. 7H). In addition, in the absence of SynCAMs, collaterals were found to extend ventrally from the dorsolateral funiculus (Fig. 7I–K). In GFP-expressing control embryos, ventrally projecting collaterals originated from more medial positions in the dorsal funiculus (Fig. 7L). Aberrantly projecting collaterals were also found in the ventral-most part of

Journal of Cell Science (2014) 127, 5288–5302 doi:10.1242/jcs.157032

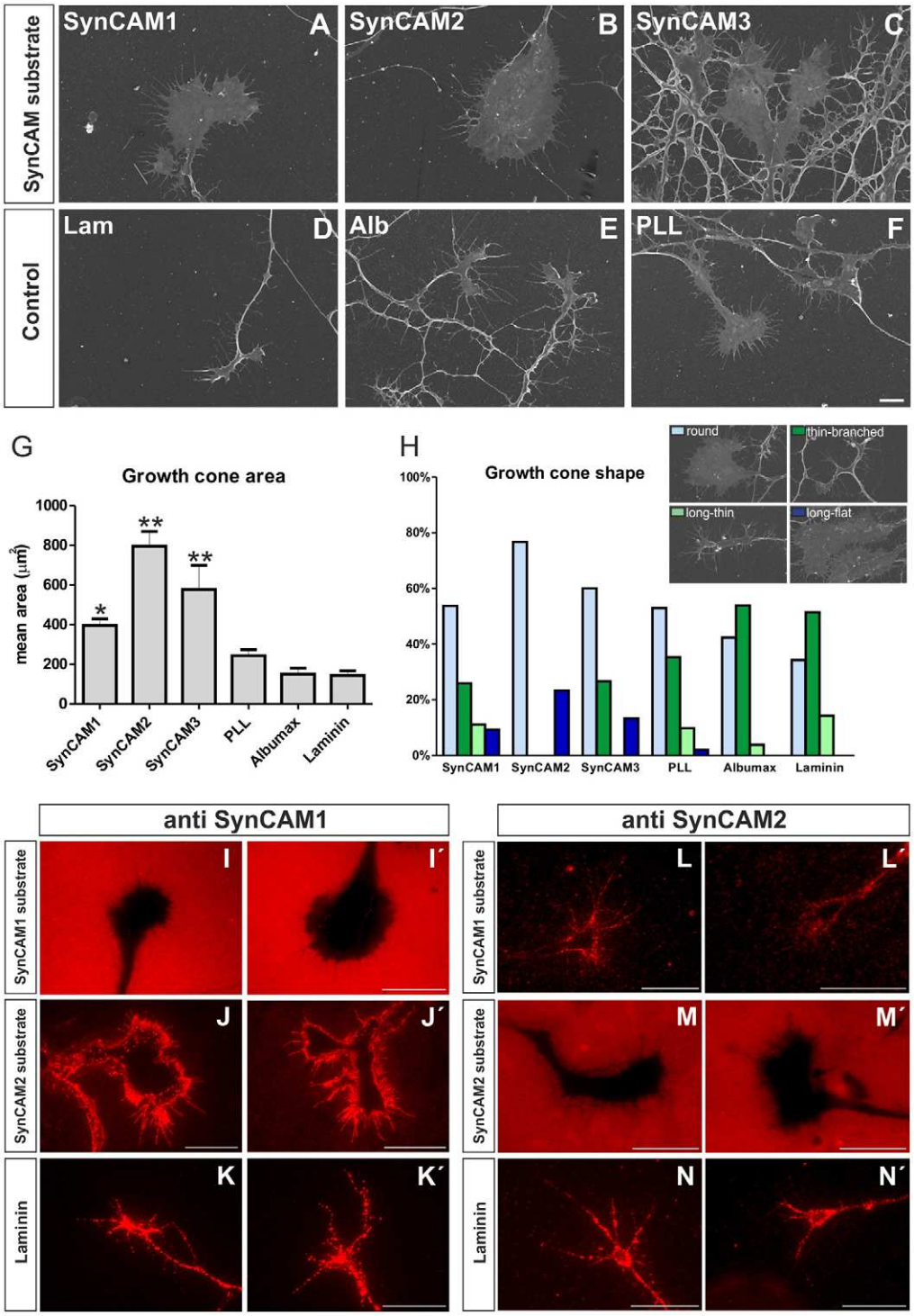

Fig. 5. SynCAM substrates affect growth cone morphology and relocate SynCAMs on the growth cone surface. Scanning electron micrographs of growth cones cultured on SynCAM1 (A), SynCAM2 (B), SynCAM3 (C), laminin (D), Albumax (E) and poly-lysine (F) were compared for size and morphology. Growth cones were markedly enlarged on SynCAM substrates compared to control substrates (G). Between 30 and 50 growth cones per condition were quantified (except SynCAM3, $n=15$). *$P<0.05$, **$P<0.01$ for the comparison between SynCAMs and control substrates (ANOVA with Tukey's post-hoc test). Values on SynCAM1 were significant in comparison to Albumax and laminin but not poly-lysine. Values are given as mean±s.e.m. (H) Growth cones were scored as showing one of four morphologies: round (light blue), thin and branched (dark green), long and thin (light green), or long and flat (dark blue). Surface staining of SynCAM1 (I,I′,J,J′,K,K′) and SynCAM2 (L,L′,M,M′,N,N′) on growth cones cultured on SynCAM1 (I,I′,L,L′), SynCAM2 (J,J′,M,M′) and laminin (K,K′,N,N′). SynCAM1 and SynCAM2 were redistributed to the substrate-facing surface of the growth cone on a SynCAM substrate (I-M). On laminin, SynCAM1 and SynCAM2 were present on the apical surface (K,N). Note that on SynCAM2 (J,J′) and SynCAM1 (L,L′) substrate, SynCAM1 and SynCAM2 are detectable at the outer rim and the filopodia of the growth cones. Neurons were stained before fixation to detect surface-expressed proteins only. Two different growth cones per condition are shown. Scale bars: 10 μm (A-F), 20 μm (I–N).

the dorsal funiculus. They were even found to cross the ventral midline (Fig. 7M–O). Collaterals crossing the ventral midline were never observed in control embryos.

In summary, these results demonstrate that SynCAMs are involved in the spinal cord entry of sensory axons, as well as the targeting of their collaterals at later stages.

DISCUSSION

Originally, SynCAMs were only implicated in late steps of neural circuit formation, such as synaptogenesis and myelination. However, we demonstrated more recently that these molecules were necessary for the guidance of post-crossing commissural axons (Niederkofler et al., 2010). In line with these findings, our study supports a role of SynCAMs in sensory axon guidance as they are required for proper entry of afferents into the DREZ and subsequent targeting of collaterals in the gray matter of the spinal cord. Taken together, our *in vitro* and *in vivo* studies support a mechanism by which SynCAM-mediated selective axon–axon contacts are required for proper axonal sorting during sensory neural circuit formation.

Journal of Cell Science (2014) 127, 5288–5302 doi:10.1242/jcs.157032

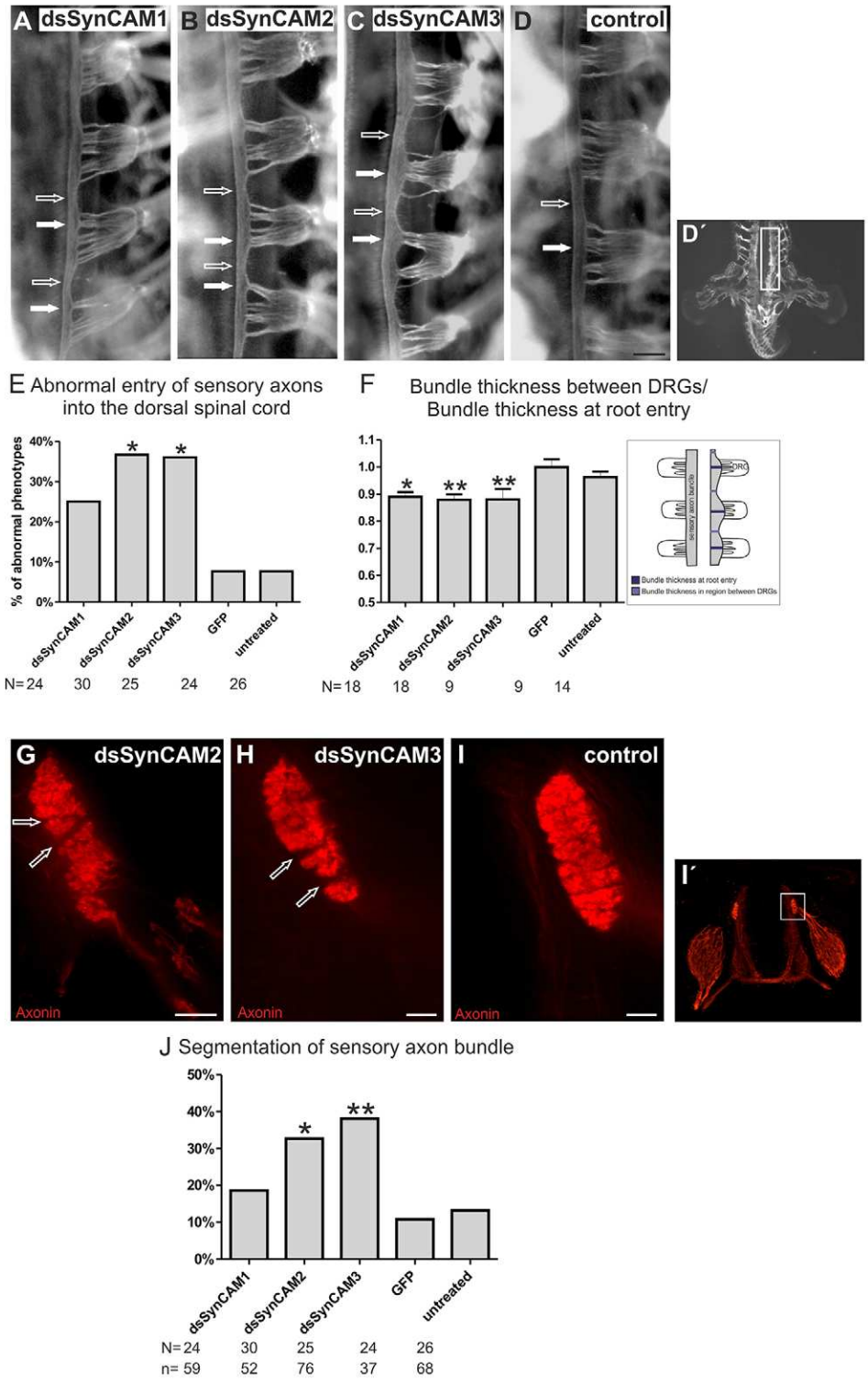

Fig. 6. SynCAMs are required for pathfinding of sensory axons. Downregulation of SynCAM1 (A), SynCAM2 (B), and SynCAM3 (C) [by use of double-stranded RNA (ds)] interfered with the normal entry of sensory afferents into the dorsal spinal cord. The longitudinal axon bundle was thicker where dorsal roots entered (white arrows) compared to the region between DRG (open arrows). A homogenous thickness along the anterior-posterior axis was seen in control embryos (D). The area shown in A-D is shown in a lower magnification image in D′. Significantly more embryos with abnormal entry of sensory axons into the dorsal spinal cord were observed after knockdown of SynCAM2 and SynCAM3 (E). Downregulation of SynCAM1 only resulted in a trend to more aberrant phenotypes but the value was not significantly different from controls. (F) The ratio of bundle thickness in the region between DRG (light purple in scheme) and at the dorsal root entry sites (dark purple) was significantly reduced after knockdown of each SynCAM family member compared to control-injected (GFP) embryos. The schematic drawing depicts where the thickness of the axon bundle was measured. After downregulation of SynCAM2 (G) and SynCAM3 (H), significantly more sensory axons bundles, stained with anti-axonin1 antibody, were segmented compared to SynCAM1 (not shown) and control embryos (I). (J) A quantification of the results shown in G–I. *$P<0.05$, **$P<0.01$ [two-tailed Fisher exact probability test (E,J) or ANOVA with Tukey's post-hoc test (F) for the comparison between experimental and GFP-expressing control groups]. Values in F are given as mean±s.e.m. N, number of embryos; n, number of DRG entry zones. Scale bars: 100 μm (A–D); 25 μm (G–I).

Complex cis- and trans-interaction patterns between SynCAMs could mediate differences in intracellular signaling

As suggested for their role in synaptogenesis and synaptic plasticity, SynCAMs assemble in cis to form dimers or oligomers (Fogel et al., 2011). So far, only homophilic cis-complexes have been reported, whereas trans-interactions were shown to be homophilic or heterophilic. Heterophilic adhesion was found to be stronger than homophilic interactions (Fogel et al., 2007; Maurel et al., 2007; Niederkofler et al., 2010; Thomas et al., 2008).

However, our detailed binding studies, including cell-based binding assays and chemical cross-linking, clearly indicated the existence of heterophilic cis-complexes (Fig. 1). Interestingly, the affinity for trans-interactions differed for heterophilic compared to homophilic cis-complexes. (Fig. 1G). These findings are not without precedent. The analysis of the interaction between the IgSF-CAMs axonin 1 and NgCAM (also known as L1CAM) provided similar results (Stoeckli et al., 1996; Buchstaller et al., 1996; Kunz et al., 1998). A cis-interaction between growth cone axonin1 and NgCAM

Journal of Cell Science (2014) 127, 5288–5302 doi:10.1242/jcs.157032

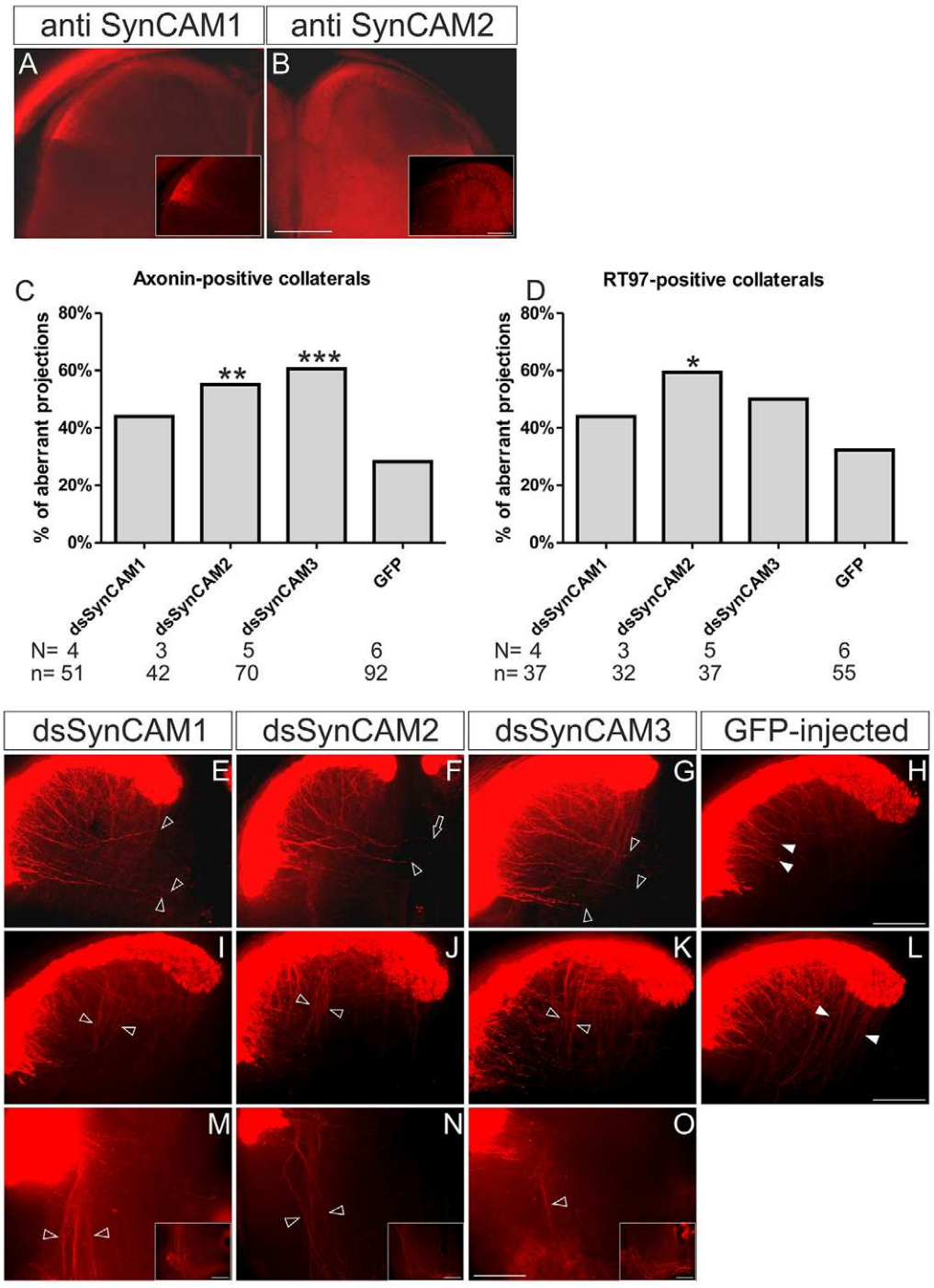

Fig. 7. Knockdown of SynCAMs results in aberrant trajectories of sensory collaterals into the gray matter of the spinal cord. The expression of SynCAM1 (A) and SynCAM2 (B) in the dorsal funiculus of HH36 spinal cord slices is complementary. SynCAM1 was expressed in the lateral dorsal funiculus and in collaterals projecting horizontally in the dorsal horn. SynCAM2 was found on afferents in the medial dorsal funiculus and on collaterals projecting to the ventral horn. Insets show higher magnification of the dorsal funiculus and collaterals. Knockdown of SynCAMs resulted in aberrant projections of axonin-1-positive (C) and RT97-positive collaterals (D) into the gray matter of the spinal cord. *$P<0.05$, **$P<0.01$, ***$P<0.001$ (two-tailed Fisher exact probability test indicated for the comparison between experimental and GFP-injected control groups). (E-O) Aberrant phenotypes of sensory collaterals observed after downregulation of SynCAM1 (E,I,M), SynCAM2 (F,J,M) and SynCAM3 (G,K,O) compared to control-treated embryos (H,L). Collaterals projected deeper into the gray matter (E-G, open arrowheads) compared to controls (H, white arrowheads). Some collaterals even crossed the midline (F, arrow). In addition, ventrally projecting collaterals extended from aberrant lateral positions in the absence of SynCAMs (I-K, open arrowheads). In GFP-injected embryos proprioceptive collaterals extended correctly from the medial dorsal funiculus (L, white arrowheads). In experimental embryos, fibers were found to leave the ventral-most part of the dorsal funiculus and to project ventrally. Many of these fibers crossed the ventral midline (M-O, open arrowheads). Such trajectories were never seen in control-treated and untreated control embryos. Insets in M-O depict the ventral part of the spinal cord including midline. HH35 vibratome sections were stained with axonin 1. N, number of embryos, n, number of sections. Scale bars: 200 μm (A,B); 100 μm (insets in A, B); 50 μm (E-O).

Journal of Cell Science (2014) 127, 5288–5302 doi:10.1242/jcs.157032

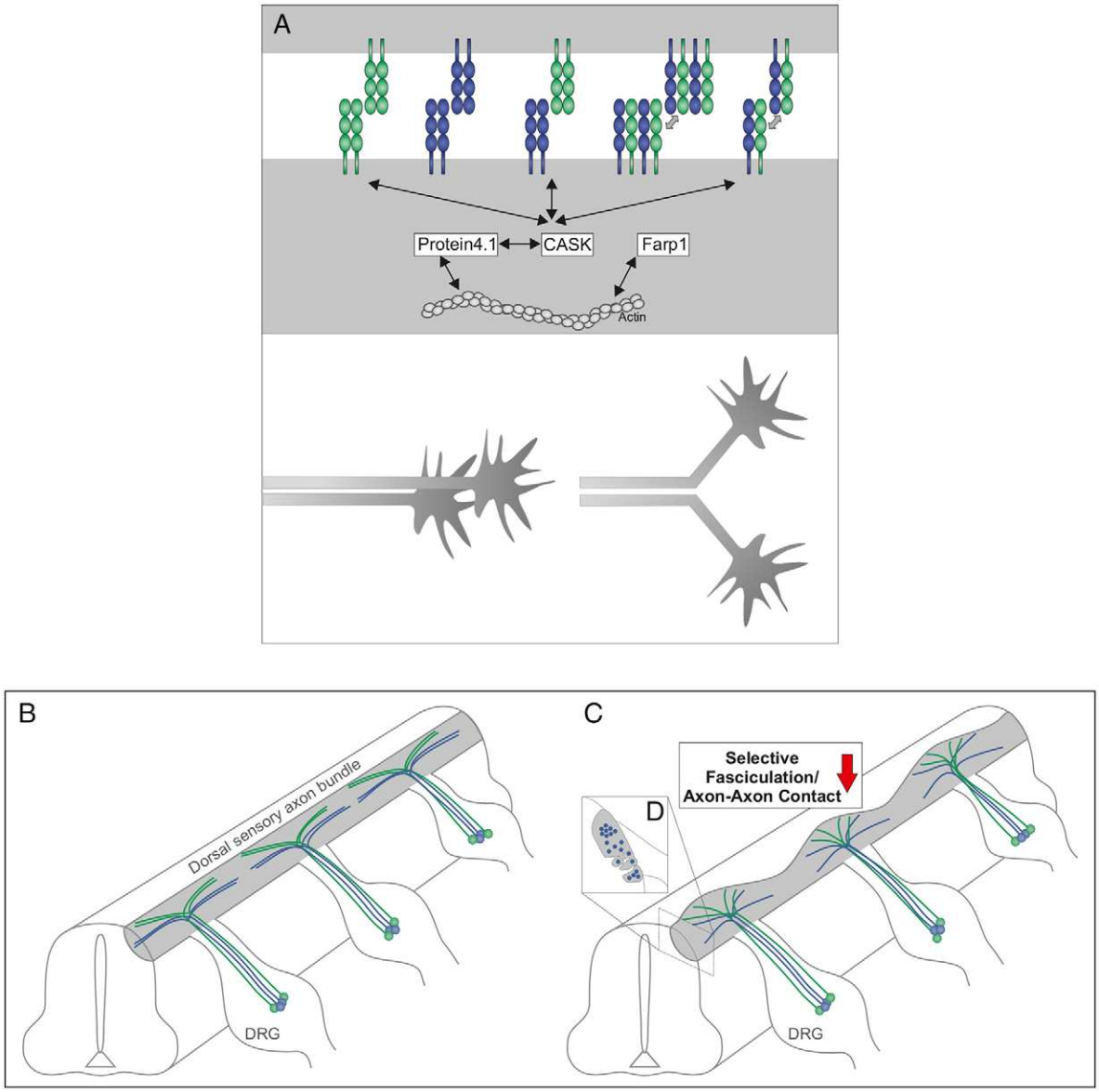

Fig. 8. Complex SynCAM interactions in cis and trans regulate axonal behavior at choice points. (A) SynCAMs form homophilic and heterophilic cis-complexes. These complexes interact in trans with cis-complexes from neighboring cells. Depending on the composition of the cis-complexes the affinity for trans-interaction partners differs. This in turn affects intracellular signaling, as different SynCAMs recruit specific intracellular scaffold and effector molecules to contact sites, and thus might change the behavior of axons at choice points (for a recent review, see Frei and Stoeckli, 2014). (B–D) SynCAMs are required for pathfinding of sensory afferents at the DREZ. (B) Sensory neurons located in the DRG extend their axons towards the spinal cord. Upon entry, axons bifurcate to grow along the anterior-posterior axis. Selective axon–axon contacts result in distinct fascicles along the longitudinal axis. In contrast, after perturbation of SynCAM expression, axon–axon contacts were altered and as a consequence axons no longer formed distinct bundles (C). In transverse sections the sensory axon bundle was segmented owing to gaps between axon sub-bundles (D).

was found to mediate axon growth on axonin1 and NgCAM substrates. As found for SynCAMs (this study), the cis-interaction of axonin 1 and NgCAM changed the binding affinity in trans (Kunz et al., 1998) as well as intracellular signaling (Kunz et al., 1996). Thus, like other IgSF-CAMs, SynCAMs could modulate intracellular signaling dependent on cis- and trans-interaction partners.

As shown for axonin1, NgCAM, and NrCAM, specific cis- and trans-interactions between SynCAMs contribute to axon guidance (Niederkofler et al., 2010; this study). In contrast to axonin1 (Stoeckli et al., 1991), NgCAM (Kuhn et al., 1991), and NrCAM (Lustig et al., 1999), SynCAMs do not strongly promote sensory axon growth (Fig. 3). However, a role on axon guidance but not growth has been found previously, as it has been shown that axonin1 is required for guidance but not growth of commissural axons (Fitzli et al., 2000).

Taken together, the results of our binding studies support the notion that IgSF-CAMs are axon guidance molecules that mediate specific signaling in response to selective cis- and trans-interactions (Stoeckli, 2004). Along these lines, studies at the synapse and with non-neuronal cells demonstrated that SynCAMs associate with different intracellular binding partners including proteins of the MAGUK family, such as CASK, Dlg3 and Pals2, members of the protein 4.1 family and the guanine nucleotide exchange factor Farp1 (Frei and Stoeckli, 2014;

Journal of Cell Science (2014) 127, 5288–5302 doi:10.1242/jcs.157032

Cheadle and Biederer, 2012; Hoy et al., 2009; Kakunaga et al., 2005; Shingai et al., 2003; Yageta et al., 2002; Zhou et al., 2005). The complex cis- and trans-interaction pattern and the resulting SynCAM complexes might recruit different intracellular effector molecules, thereby eliciting specific responses and, thus, fine-tune the behavior of axons and their growth cones (Fig. 8A).

SynCAMs regulate selective contact and fasciculation between sensory axons

Based on our model, specific intracellular SynCAM-derived signaling is dependent on the formation of different cis- and trans-interaction complexes. Changing the levels of SynCAM expression would therefore alter the composition of SynCAM complexes, which in turn could result in changes of the behavior of axons and growth cones. Indeed, our *in vitro* and *in vivo* results support this hypothesis. Both adding SynCAM externally as a substrate and perturbing endogenously expressed SynCAM in DRG resulted in altered axon–axon contacts, as we observed increased crossing of axons between fascicles (Fig. 4; supplementary material Fig. S3).

Changes in growth cone morphology and SynCAM distribution suggest an active contribution of SynCAMs to guidance decisions at choice points

In agreement with a role in axon guidance, SynCAMs affect the morphology of growth cones and the distribution of surface molecules (Fig. 5). Similar to sensory neurons on Pals2 and NgCAM substrate (Stoeckli et al., 1996; Buchstaller et al., 1996; Kunz et al., 1998), SynCAMs were redistributed on the growth cone surface in a substrate-dependent manner and like on axonin 1, growth cones on SynCAM were found to be much larger than those on laminin (Fig. 5). Axonin 1 was found to relocate to the substratum-facing surface of the growth cone in response to a cis-interaction with NgCAM (Stoeckli et al., 1996; Buchstaller et al., 1996). The formation of specific cis-interactions was found to affect intracellular signaling (Kunz et al., 1996; Kunz et al., 1998). Thus, specific cis-interactions and the resulting modulation of trans-interaction allow for changes in axonal behavior at choice points (Fig. 8A). This was shown previously for commissural axons at the floorplate (Niederkofler et al., 2010). In this study, we show that this holds true also for sensory afferents in the DREZ (Fig. 6; Fig. 7; Fig. 8B–D). Again, these findings for SynCAMs are in agreement with previous observations made with IgSF-CAMs of the contactin and the L1 family (Stoeckli, 2004 and Stoeckli, 2010). Specific interactions between axonin1 and NgCAM, and between contactin 1 (also known as F11) and NrCAM were shown to be required for pathfinding of nociceptive and proprioceptive afferents and collaterals, respectively (Perrin et al., 2001).

Etiologies of neurodevelopmental diseases go beyond defective synapses

Recently, two missense mutations in SynCAM1 have been found in patients diagnosed with autism spectrum disorder (ASD) (Zhiling et al., 2008). So far neurodevelopmental disorders have been linked to defective synaptogenesis and deficits in synaptic plasticity. However, our results demonstrate that SynCAMs are important early on in neural circuit formation and therefore suggest that the underlying pathology of neurodevelopmental diseases could involve earlier steps than aberrant synapse formation and plasticity. Indeed, changes in axonal connectivity have been associated with autism (Geschwind and Levitt, 2007), supporting the idea that disrupted axonal pathfinding contributes to the etiology of neurodevelopmental diseases.

Conclusion

In summary, our *in vitro* and *in vivo* studies demonstrate a role of SynCAMs in early aspects of neural circuit formation, complementing published results on their role in myelination, synapse formation and synaptic plasticity. Many of the characteristics of SynCAM interactions are shared with other IgSF-CAMs. The composition of SynCAM cis-clusters affects the selection of trans-interactions and the intracellular signaling cascade. Thus, SynCAMs play an active role in axon-axon or axon-intermediate target contact during axon guidance.

MATERIALS AND METHODS

Recombinant SynCAM proteins and antibodies

Plasmids encoding the ectodomains of chicken SynCAM1 and SynCAM2 fused to AP-myc-6xHis tag of the pAPtag5 vector (Niederkofler et al., 2010) were transfected into HEK293T cells for the generation of SynCAM ectodomains that were used for in vitro binding studies. To obtain SynCAMs used as antigens and substrate, plasmids encoding the ectodomains of chicken SynCAM1, chicken SynCAM2, and human SynCAM3 were fused to a 6xHis-STOP and cloned into the pAPtag5 vector. HEK293T cells were transfected with plasmids using standard calcium-phosphate precipitation. After 24 hours, the medium was changed to serum-free medium (OptiMEM, Gibco). The supernatant was collected 48 hours later and the SynCAM fusion proteins were purified by affinity chromatography (FPLC) using Ni-NTA agarose beads (Macherey-Nagel, Dueren, Germany). The purity of the ectodomains was confirmed on a silver-stained gel and by western blotting using mouse anti-Myc or rabbit anti-His antibodies and sheep anti-mouse-HRP or goat anti-rabbit-HRP antibodies (supplementary material Table S1), respectively. Antibodies against the ectodomains of the different SynCAMs were produced by injecting rabbits with 50 µg SynCAM1 or SynCAM3, respectively, or 30 µg SynCAM2. At least three booster injections were given at six-week intervals. Specificity of the antibodies was assessed on western blots (supplementary material Fig. S1,F-J). The antibody raised against human SynCAM3 recognized the human protein but a variety of unspecific bands in lysates of chicken spinal cords and DRG (data not shown). Therefore, we could not use this antibody for staining or binding assays. Sources and dilutions of primary and secondary antibodies used for immunostaining and western blots are given in supplementary material Table S2.

Binding assays

HeLa cells, plated at a density of 20,000 or 30,000 cells per cm^2 in LabTeks (Nunc, Rochester, NY, US), were either single- or co-transfected with full-length pcDNA3.1-SynCAM1-HA or -Flag and pCAGGs-SynCAM2-HA or -Flag constructs or empty vectors using Lipofectamine 2000 (Invitrogen, Carlsbad, CA, US). To keep the total amount of transfected DNA constant (400 ng/well), we co-transfected 200 ng of empty vector for single transfection. For the trans-binding assay, cells were separately transfected with HA- or Flag-tagged SynCAM1 and SynCAM2. After 24 hours the different cell populations were mixed 1:1. SynCAM ectodomains were added 24 hours post-transfection or 24 hours after mixing the differently transfected cell populations at a final concentration of 10 µg/ml in OptiMEM (Gibco, Carlsbad, CA, US) for 90 minutes at 4°C. Cells were fixed in 4% formaldehyde, and permeabilized with 0.1% Triton-X100 for 15 minutes before staining. For the quantification of the binding strength, random images were taken with an Olympus BX61 microscope and a Hamamatsu ORCA-R2 camera (Hamamatsu, Japan) using the same settings (exposure time, upper/lower limit). The fluorescent intensities were measured with ImageJ. The binding strength of ectodomains to single- and co-transfected cells was calculated by the intensity ratios of the ectodomains (Myc-signal) to the transfected SynCAMs (either Flag- or HA-signal).

Co-immunoprecipitation

HEK293T were co-transfected with full-length pcDNA3.1-SynCAM1-myc/his or pcDNA3.1-SynCAM1-HA and pCAGGs-SynCAM2-HA or -Flag (Niederkofler et al., 2010) and empty vectors using standard calcium-phosphate precipitation. After 24 hours, cells were lysed in 150 mM NaCl and 1% Triton X-100 in 20 mM Tris-HCl pH 8.0, supplemented with

protease inhibitors (Roche, Basel, Switzerland). Lysates were incubated with agarose beads coupled to anti-Myc (Thermo Scientific, Waltham, MA), anti-HA (Sigma, St. Louis, MO) and anti-Flag antibodies (Sigma) for 2 hours at 4℃ on an orbital shaker. Proteins bound to the anti-Myc-matrix were eluted at pH 2.8 (ProFound c-Myc-Tag IP/Co-IP Kit #23620, Thermo Scientific) followed by immediate neutralization with 1 M Tris-HCl pH 9.5, added to a final concentration of 150 mM. Proteins bound to anti-HA- and anti-Flag-matrix were eluted with 100 µg/ml HA- and Flag peptides (Sigma), respectively. For transfection control, cells were lysed in 2% SDS, 10% glycerol, 6 M urea and 5% mercaptoethanol in 62.5 mM Tris-HCl pH 6.8. For immunoprecipitation of endogenously expressed SynCAMs, DRG of E5 chicken embryos were dissected and cultured as explants on poly-lysine and laminin-coated dishes. After 48 hours, DRG were lysed in 180 mM NaCl, 5 mM EDTA and 1% Triton X-100 in 50 mM Tris-HCl pH 8, supplemented with protease inhibitors, and homogenized. Lysates were preabsorbed with protein-A–sepharose (GE Healthcare, Buckinghamshire, UK) for 1 hour at 4℃ on an orbital shaker. After removing the beads, 30 µg of SynCAM1 IgGs or SynCAM2 serum were added to the lysates for 2 hours to overnight at 4℃ followed by incubation with protein-A–Sepharose for another hour at 4℃. Proteins bound to the beads were eluted by boiling (95℃) for 5 minutes in 2× sample buffer containing 4% SDS, 20% glycerol, 0.04% Bromophenol Blue and 100 mM DTT in 125 mM Tris-HCl pH 6.8.

Chemical cross-linking assay

One day after transfection with pcDNA3.1-SynCAM1-HA, pcDNA3.1-SynCAM1-Flag or pCAGGs-SynCAM2-Flag (see above), cells were rinsed and detached with 5 mM EDTA in 10 mM phosphate buffer containing 137 mM NaCl, 3 mM KCl, pH 8.0. Single cells obtained by trituration were plated at a density of 300,000 cells per 10-cm dish. Six hours later, cells were carefully rinsed in phosphate buffer without EDTA on ice. For cross-linking, cells were incubated with 1 mM bis-sulfosuccinimidyl suberate (BS^3; Thermo Scientific) for 1 hour at 4℃ while gently shaking. The reaction was quenched by adding 1 M Tris-HCl pH 7.5, to a final concentration of 20 mM for 15 minutes at room temperature. Cell lysis was as described above. For co-immunoprecipitation, anti-HA-matrix was used and proteins were eluted in 2×sample buffer (see above).

In situ hybridization

DIG-labeled *in situ* hybridization probes were produced from ChEST583g11 (SynCAM1), ChEST114o11 (SynCAM2) and CHEST478g10 (SynCAM3) obtained from Source BioScience LifeSciences (Cambridge, UK). *In situ* hybridization was performed as described previously (Mauti et al., 2006). Sections were hybridized with 0.75 ng/µl anti-sense and sense probes.

Cultures of DRG sensory neurons

Single cells or intact DRG were collected from either E5 (HH25 or HH26) or E8 (HH34) chicken embryos and cultured as described (Stoeckli et al., 2013; Niederkofler et al., 2010). LabTeks were precoated with 10 µg/ml poly-lysine (Sigma) followed by coating with either 10 µg/ml Laminin (Invitrogen), $SynCAM1^{ecto}$ or $SynCAM2^{ecto}$ as described previously (Stoeckli et al., 2013). Dissociated sensory neurons were cultured at a density of 10,000 to 20,000 cells per cm^2 for 48 hours. For surface staining, antibodies were directly added to the medium for 45 minutes at 4℃ before fixation.

For the choice assay (Niederkofler et al., 2010), 15,000 COS cells per cm^2 were transfected with full-length pcDNA3.1-SynCAM1-HA, pCAGGs-SynCAM2-HA, pcDNA3.1-humanSynCAM3-HA and pcDNA3-MARCKS-GFP. After 24 hours, 2,000 dissociated sensory neurons were added to the COS7 cell layer. After 24 hours, neurons were visualized with anti-neurofilament staining (supplementary material Table S2).

For the outgrowth assay poly-lysine-precoated LabTek dishes were coated with 0.4 µg/ml, 10 µg/ml and 50 µg/ml SynCAMs or Albumax (Gibco) as described previously (Stoeckli et al., 2013). To obtain low-density cultures, 4000 sensory neurons per cm^2 were cultured for 28 or 48 hours. Neurite lengths were quantified as described earlier (Stoeckli et al., 1991) using CellM software (Olympus). For both assays, images were taken randomly with a fluorescence microscope (Olympus BX51) and an Olympus XC30 camera.

In ovo RNA interference

In ovo RNA interference (RNAi) was used to silence genes of interest as described previously (Pekarik et al., 2002; Mauti et al., 2007). In brief, a solution containing 300–500 ng/µl of long dsRNA together with a GFP reporter plasmid under the control of the β-actin promotor (20 or 50 ng/µl) was injected into the central canal of E2 chicken embryos (HH12-HH15) followed by electroporation to efficiently target DRG. For the generation of long double-stranded RNA (dsRNA) the same ChESTs as for the *in situ* probes were used, except of ChEST96i3 (SynCAM2). DsRNA was prepared as previously described (Pekarik et al., 2002). All dsRNAs were derived from 600–800 bp in the 3′UTR of the corresponding SynCAM mRNA. The efficiency and specificity of the dsRNA *in vivo* was demonstrated previously (Niederkofler et al., 2010). Here, we used an *in vitro* method to demonstrate efficiency and specificity of SynCAM knockdown. Long dsRNA against the different SynCAMs was digested into siRNA by ShortCut RNaseIII (New England BioLabs, Ipswich, MA) for 20 minutes at 37℃. HEK293T cells were plated for 24 hours at a density of 40,000 cells per well of the LabTek dish and triple-transfected using Lipofectamine 2000 (Invitrogen) with 50 ng/well destabilized GFP fused to the 3′UTR of SynCAMs (Niederkofler et al., 2010), 50 ng/well of the different siRNAs, and 50 ng/well of a construct encoding tomato-fluorescent protein as transfection control. Random pictures were taken with constant settings (exposure time, upper limit). For quantification the intensity of the GFP signal was normalized to the intensity of the Tomato signal (ImageJ). SynCAM1 levels were reduced by 93.7%, SynCAM2 by 99.3%, and SynCAM3 by 93.2%. All experiments including animals were carried out in accordance with Swiss law on animal experimentation and approved by the cantonal veterinary office of Zurich.

Preparation of intact DRG explants for scanning electron microscopy analysis

Intact DRG were cultured on 12-mm round poly-lysine-precoated coverslips coated with 10 µg/ml SynCAM1, SynCAM2, SynCAM3, Albumax, laminin or collagen (66.7 µg/ml; Millipore, Billerica, MA). For the analysis of DRG lacking SynCAMs, *in ovo* RNAi in E2 chicken embryos was performed as described above. After 48 hours, DRG were fixed in 2.5% glutaraldehyde and 0.8% formaldehyde in 0.1 M phosphate buffer pH 7.4, for 20 minutes to one hour at room temperature or overnight at 4℃. Samples were incubated with 1% osmium tetroxide in 0.1 M phosphate buffer pH 7.4, for 30 minutes on ice followed by dehydration in a graded ethanol series (70% to 100%). Samples were prepared by critical-point drying followed by platinum and carbon coating. Images were taken from the periphery of the axonal network with a Zeiss Supra 50 VP scanning electron microscope. Growth cone areas and neurite lengths were measured with the CellM software. Filopodia along neurites were counted and normalized to neurite length. Growth cones were classified blind to the experimental condition into four different shape groups: round, thin and branched, long and thin, and long and flat. Measurements were taken from two independent experiments. Per condition we used at least two different embryos for DRG explants.

Immunohistochemistry and whole-mount staining

For staining, 25-µm-thick cryostat sections of HH25 or HH26 chicken and E12.5 mouse spinal cords and 250-µm-thick vibratome slices of HH25 or HH26, and HH35 or HH36 chicken spinal cords were permeabilized with 0.1% or 0.3% Triton X-100, respectively. Cryosections and vibratome slices were stained with rabbit anti-SynCAM or rabbit anti-axonin1 antibodies (supplementary material Table S2). In some experiments, slices were co-stained with RT97 (supplementary material Table S2). Whole-mount staining was performed as described previously (Mauti et al., 2007).

Quantification of sensory axon phenotypes

Trajectories of sensory axons and their collaterals were analyzed in HH35 vibratome slices, in HH25 or HH26 whole-mount embryos stained with an anti-neurofilament antibody or by tracing with DiI by a person blind to the experimental condition. Images of whole-mount embryos were taken with an Olympus SZX12 equipped with a KAPPA CF8/4 camera. DiI-labeled afferents were imaged with an inverted microscope (Olympus IX70) and an Olympus ColorView 2 camera. Sensory afferents and

collaterals in vibratome slices were analyzed using an Olympus BX51 microscope/Olympus XC30 camera and an Olympus BX61 microscope/Hamamatsu ORCA-R2 camera, respectively. For quantification of the axon bundle thickness the thickest region at the level of the roots and the thinnest region between two DRG were measured using ImageJ software. The average of the ratios per embryo and per group was calculated and compared to the ratio of GFP-injected control embryos.

Statistical analysis

For statistical analysis of the whole-mount embryos and vibratome slices, the two-tailed Fisher exact probability test was used. For statistical analysis of *in vitro* experiments, the two-tailed Student's *t*-test or one-way ANOVA followed by the Tukey's post-hoc test were used to calculate *P*-values using Microsoft Excel 2007 or vassarstats.net, respectively. *P*-values lower than 0.05 were considered statistically significant (*$P<0.05$, **$P<0.01$, ***$P<0.001$). Values represent the mean±s.e.m.

Acknowledgements

We thank laboratory members for helpful comments and discussion, Beat Kunz (University of Zurich) for help with protein purification, Andres Käch and Gery Barmettler from the Center for Microscopy and Image Analysis of the University of Zurich for help with electron microscopy.

Competing interests

The authors declare no competing interests.

Author contributions

J.F., I.A. and E.S. carried out the experiments, M.G. helped with cloning, J.F. and E.S. designed the studies and wrote the manuscript.

Funding

This project was supported by a grant from the Swiss National Science Foundation.

Supplementary material

Supplementary material available online at
http://jcs.biologists.org/lookup/suppl/doi:10.1242/jcs.157032/-/DC1

References

Biederer, T., Sara, Y., Mozhayeva, M., Atasoy, D., Liu, X., Kavalali, E. T. and Südhof, T. C. (2002). SynCAM, a synaptic adhesion molecule that drives synapse assembly. *Science* **297**, 1525-1531.

Buchstaller, A., Kunz, S., Berger, P., Kunz, B., Ziegler, U., Rader, C. and Sonderegger, P. (1996). Cell adhesion molecules NgCAM and axonin-1 form heterodimers in the neuronal membrane and cooperate in neurite outgrowth promotion. *J. Cell Biol.* **135**, 1593-1607.

Cheadle, L. and Biederer, T. (2012). The novel synaptogenic protein Farp1 links postsynaptic cytoskeletal dynamics and transsynaptic organization. *J. Cell Biol.* **199**, 985-1001.

Eide, A. L. and Glover, J. C. (1995). Development of the longitudinal projection patterns of lumbar primary sensory afferents in the chicken embryo. *J. Comp. Neurol.* **353**, 247-259.

Eide, A. L. and Glover, J. C. (1997). Developmental dynamics of functionally specific primary sensory afferent projections in the chicken embryo. *Anat. Embryol. (Berl.)* **195**, 237-250.

Fitzli, D., Stoeckli, E. T., Kunz, S., Siribour, K., Rader, C., Kunz, B., Kozlov, S. V., Buchstaller, A., Lane, R. P., Suter, D. M. et al. (2000). A direct interaction of axonin-1 with NgCAM-related cell adhesion molecule (NrCAM) results in guidance, but not growth of commissural axons. *J. Cell Biol.* **149**, 951-968.

Fogel, A. I., Akins, M. R., Krupp, A. J., Stagi, M., Stein, V. and Biederer, T. (2007). SynCAMs organize synapses through heterophilic adhesion. *J. Neurosci.* **27**, 12516-12530.

Fogel, A. I., Stagi, M., Perez de Arce, K. and Biederer, T. (2011). Lateral assembly of the immunoglobulin protein SynCAM 1 controls its adhesive function and instructs synapse formation. *EMBO J.* **30**, 4728-4738.

Frei, J. A. and Stoeckli, E. T. (2014). SynCAMs extend their functions beyond the synapse. *Eur. J. Neurosci.* **39**, 1752-1760.

Fujita, E., Dai, H., Tanabe, Y., Zhiling, Y., Yamagata, T., Miyakawa, T., Tanokura, M., Momoi, M. Y. and Momoi, T. (2010). Autism spectrum disorder is related to endoplasmic reticulum stress induced by mutations in the synaptic cell adhesion molecule, CADM1. *Cell Death Dis.* **1**, e47.

Geschwind, D. H. and Levitt, P. (2007). Autism spectrum disorders: developmental disconnection syndromes. *Curr. Opin. Neurobiol.* **17**, 103-111.

Hoy, J. L., Constable, J. R., Vicini, S., Fu, Z. and Washbourne, P. (2009). SynCAM1 recruits NMDA receptors via protein 4.1B. *Mol. Cell. Neurosci.* **42**, 466-483.

Kakunaga, S., Ikeda, W., Itoh, S., Deguchi-Tawarada, M., Ohtsuka, T., Mizoguchi, A. and Takai, Y. (2005). Nectin-like molecule-1/TSLL1/SynCAM3: a neural tissue-specific immunoglobulin-like cell-cell adhesion molecule localizing at non-junctional contact sites of presynaptic nerve terminals, axons and glia cell processes. *J. Cell Sci.* **118**, 1267-1277.

Kuhn, T. B., Stoeckli, E. T., Condrau, M. A., Rathjen, F. G. and Sonderegger, P. (1991). Neurite outgrowth on immobilized axonin-1 is mediated by a heterophilic interaction with L1(G4). *J. Cell Biol.* **115**, 1113-1126.

Kunz, S., Ziegler, U., Kunz, B. and Sonderegger, P. (1996). Intracellular signaling is changed after clustering of the neural cell adhesion molecules axonin-1 and NgCAM during neurite fasciculation. *J. Cell Biol.* **135**, 253-267.

Kunz, S., Spirig, M., Ginsburg, C., Buchstaller, A., Berger, P., Lanz, R., Rader, C., Vogt, L., Kunz, B. and Sonderegger, P. (1998). Neurite fasciculation mediated by complexes of axonin-1 and Ng cell adhesion molecule. *J. Cell Biol.* **143**, 1673-1690.

Lustig, M., Sakurai, T. and Grumet, M. (1999). Nr-CAM promotes neurite outgrowth from peripheral ganglia by a mechanism involving axonin-1 as a neuronal receptor. *Dev. Biol.* **209**, 340-351.

Maurel, P., Einheber, S., Galinska, J., Thaker, P., Lam, I., Rubin, M. B., Scherer, S. S., Murakami, Y., Gutmann, D. H. and Salzer, J. L. (2007). Nectin-like proteins mediate axon Schwann cell interactions along the internode and are essential for myelination. *J. Cell Biol.* **178**, 861-874.

Mauti, O., Sadhu, R., Gemayel, J., Gesemann, M. and Stoeckli, E. T. (2006). Expression patterns of plexins and neuropilins are consistent with cooperative and separate functions during neural development. *BMC Dev. Biol.* **6**, 32.

Mauti, O., Domanitskaya, E., Andermatt, I., Sadhu, R. and Stoeckli, E. T. (2007). Semaphorin6A acts as a gate keeper between the central and the peripheral nervous system. *Neural Dev.* **2**, 28.

Morales, G., Hubert, M., Brümmendorf, T., Treubert, U., Tárnok, A., Schwarz, U. and Rathjen, F. G. (1993). Induction of axonal growth by heterophilic interactions between the cell surface recognition proteins F11 and Nr-CAM/Bravo. *Neuron* **11**, 1113-1122.

Niederkofler, V., Baeriswyl, T., Ott, R. and Stoeckli, E. T. (2010). Nectin-like molecules/SynCAMs are required for post-crossing commissural axon guidance. *Development* **137**, 427-435.

Pekarik, V., Bourikas, D., Miglino, N., Joset, P., Preiswerk, S. and Stoeckli, E. T. (2002). Screening for gene function in chicken embryo using RNAi and electroporation. *Nat. Biotechnol.* **21**, 93-96.

Perrin, F. E., Rathjen, F. G. and Stoeckli, E. T. (2001). Distinct subpopulations of sensory afferents require F11 or axonin-1 for growth to their target layers within the spinal cord of the chick. *Neuron* **30**, 707-723.

Robbins, E. M., Krupp, A. J., Perez de Arce, K., Ghosh, A. K., Fogel, A. I., Boucard, A., Südhof, T. C., Stein, V. and Biederer, T. (2010). SynCAM 1 adhesion dynamically regulates synapse number and impacts plasticity and learning. *Neuron* **68**, 894-906.

Shingai, T., Ikeda, W., Kakunaga, S., Morimoto, K., Takekuni, K., Itoh, S., Satoh, K., Takeuchi, M., Imai, T., Monden, M. et al. (2003). Implications of nectin-like molecule-2/IGSF4/RA175/SgIGSF/TSLC1/SynCAM1 in cell-cell adhesion and transmembrane protein localization in epithelial cells. *J. Biol. Chem.* **278**, 35421-35427.

Stoeckli, E. T. (2004). Ig superfamily cell adhesion molecules in the brain. *Handb. Exp. Pharmacol.* **165**, 373-401.

Stoeckli, E. T. (2010). Neural circuit formation in the cerebellum is controlled by cell adhesion molecules of the Contactin family. *Cell Adh. Migr.* **4**, 523-526.

Stoeckli, E. T. (2012). What does the developing brain tell us about neural diseases? *Eur. J. Neurosci.* **35**, 1811-1817.

Stoeckli, E. T., Kuhn, T. B., Duc, C. O., Ruegg, M. A. and Sonderegger, P. (1991). The axonally secreted protein axonin-1 is a potent substratum for neurite growth. *J. Cell Biol.* **112**, 449-455.

Stoeckli, E. T., Ziegler, U., Bleiker, A. J., Groscurth, P. and Sonderegger, P. (1996). Clustering and functional cooperation of Ng-CAM and axonin-1 in the substratum-contact area of growth cones. *Dev. Biol.* **177**, 15-29.

Stoeckli, E. T., Kilinc, D., Kunz, B., Kunz, S., Lee, G. U., Martines, E., Rader, C. and Suter, D. (2013) Analysis of cell-cell contact mediated by Ig superfamily cell adhesion molecules. *Curr. Protoc. Cell Biol.* **61**, 9.5.1-9.5.85.

Takayanagi, Y., Fujita, E., Yu, Z., Yamagata, T., Momoi, M. Y., Momoi, T. and Onaka, T. (2010). Impairment of social and emotional behaviors in Cadm1-knockout mice. *Biochem. Biophys. Res. Commun.* **396**, 703-708.

Thomas, L. A., Akins, M. R. and Biederer, T. (2008). Expression and adhesion profiles of SynCAM molecules indicate distinct neuronal functions. *J. Comp. Neurol.* **510**, 47-67.

Yageta, M., Kuramochi, M., Masuda, M., Fukami, T., Fukuhara, H., Maruyama, T., Shibuya, M. and Murakami, Y. (2002). Direct association of TSLC1 and DAL-1, two distinct tumor suppressor proteins in lung cancer. *Cancer Res.* **62**, 5129-5133.

Zhiling, Y., Fujita, E., Tanabe, Y., Yamagata, T., Momoi, T. and Momoi, M. Y. (2008). Mutations in the gene encoding CADM1 are associated with autism spectrum disorder. *Biochem. Biophys. Res. Commun.* **377**, 926-929.

Zhou, Y., Du, G., Hu, X., Yu, S., Liu, Y., Xu, Y., Huang, X., Liu, J., Yin, B., Fan, M. et al. (2005). Nectin-like molecule 1 is a protein 4.1N associated protein and recruits protein 4.1N from cytoplasm to the plasma membrane. *Biochim. Biophys. Acta* **1669**, 142-154.